ACS APPLIED MATERIALS & INTERFACES

Research Article

www.acsami.org

Nb–C Nanocomposite Films with Enhanced Biocompatibility and Mechanical Properties for Hard-Tissue Implant Applications

Luis Yate,[†] L. Emerson Coy,[§] Danijela Gregurec,[‡] Willian Aperador,[∥] Sergio E. Moya,[‡] and Guocheng Wang*[,‡]

[†]Surface Analysis and Fabrication Platform, CIC biomaGUNE, Paseo Miramón 182, 20009 Donostia-San Sebastian, Spain

[§]NanoBioMedical Center, Adam Mickiewicz University, Umultowska 85, 61-614 Poznan, Poland

[‡]Soft Matter Nanotechnology Laboratory, CIC biomaGUNE, Paseo Miramón 182, 20009 Donostia-San Sebastian, Spain

[∥]School of Engineering, Universidad Militar Nueva Granada, Carrera 11 #101-80, 49300 Bogotá, Colombia

ABSTRACT: One of the key challenges in engineering of orthopedic implants is to "bioactivate" their surface by using different surface techniques and materials. Carbon, especially amorphous (a-C) and diamond-like carbon down (DLC) films have attracted much attention in biomedical fields due to their biocompatibility and low coefficient of friction. However, they are unsuitable for uses as a "bioactivity enhancer" of orthopedic implants due to their bioinertness. In this work, we use the nonreactive magnetron sputtering technique to produce a-C films including the biocompatible niobium (Nb) element to alter the surface chemistry and nanotopography of the a-C films with the purpose of bioactivating the a-C film coated implants. Results show that the nanocomposite films (Nb–C) formed by the addition of Nb into the a-C films not only have improved corrosion resistance, but also possess enhanced mechanical properties (nanohardness, Young's modulus and superelastic recovery). Preosteoblasts (MC3T3-E1) cultured on the Nb–C films have enhanced adhesion and upregulated alkaline phosphatase (ALP) activity, compared to those cultured on the a-C film and TiO_2 films used as a control, which are thought to be ascribed to the combined effects of the changes in surface chemistry and the refinement of the nanotopography caused by the addition of Nb.

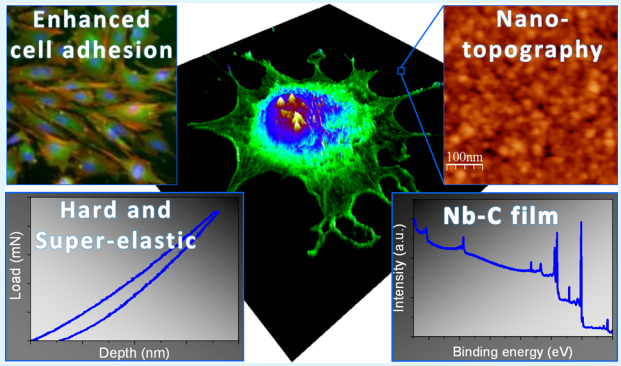

KEYWORDS: *niobium, amorphous carbon, thin films, biocompatibility, osteoblast, orthopedic implant*

INTRODUCTION

Due to the population aging and a large majority of traumatic injuries caused by accidents, demand for the orthopedic implant is ever-increasing. Many materials have been developed to replace the lost bone and restore the bone functions. Titanium (Ti) and its alloys are so far the most popular materials for this purpose due to their excellent properties such as low specific weight, high corrosion resistance and good biocompatibility.[1] However, the suboptimal surface properties in terms of bioactivity are compromising the overall performance of Ti and Ti alloy implants, resulting in a high revision rate and thus raising a burden to the patients and nations.[2,3]

The surface properties of orthopedic implants are of critical importance for their success after implantation. Among them, surface chemistry and nanotopograpy have been proved to be especially significant in enhancing the functions of osteoblasts and promoting bone tissue regeneration.[4−6] Therefore, chemical and topographical modification of the implant surface at both the micro and nanoscale becomes a dominant approach for improving the biological performance of the implants.[7,8] Carbon films, especially amorphous carbon (a-C) or diamond-like carbon (DLC), are well-known for their chemical inertness, and have been widely used for improving the hemocompatibility and biocompatibility of artificial implants in the biomedical field.[9] In addition, DLC films also show high hardness and low coefficient of friction.[9,10] Although their biocompatibility has been widely proven, these films lack bioactivity, referred as the ability to induce bone formation, which limits their use for orthopedic applications. Niobium (Nb) has received great attention in the biomedical field as an alloying element to develop new alloys. Due to the changes in the chemical composition, Nb-containing alloys such as Ti–Nb and Zr–Nb alloys have been proved to have enhanced corrosion resistance and biocompatibility.[11,12] Moreover, some studies demonstrated that the changes in surface chemistry by the incorporation of Nb enhanced the osteoblastic differentiation.[13−15] Shapira et al.[15] reported that Nb containing Ti alloys enhanced alkaline phosphatase (ALP) activity and

Received: February 6, 2015
Accepted: March 4, 2015
Published: March 4, 2015

DOI: 10.1021/acsami.5b01193
ACS Appl. Mater. Interfaces 2015, 7, 6351−6358

promoted more rapid maturation of osteoblasts, suggesting the potential of Nb in inducing osteogenic functions of osteoblast. Therefore, in this study, we intend to incorporate Nb into a-C films to enhance the bioactivity of the a-C film coated orthopedic implants. We found in our previous work that the introduction of Nb_2O_5 into plasma sprayed TiO_2 coatings induced a significant change in the nanotopography of the TiO_2 coating besides changes in surface chemistry.[16] Therefore, it is also expected in this study that the addition of Nb in the a-C film can also induce topographic alteration. As a result, maximized enhancement on the osseointegration of the implant can be obtained by synergistic effects of both the surface topography and chemistry changes.

In this work, nonreactive magnetron sputtering was used to deposit the thin films. Surface chemistry, mechanical properties and corrosion resistance of the a-C film with and without Nb were investigated and compared. Preosteoblast cells (MC3T3-E1) were used to evaluate the influences of the films on the osteoblast behaviors.

EXPERIMENTAL SECTION

Deposition of the Films. Amorphous carbon (a-C), Nb−C and TiO_2 thin films were deposited with nonreactive and reactive magnetron sputtering on silicon(100), glass and AISI 316LVM steel substrates using an AJA-ATC 1800 system with a base pressure of 10^{-7} Pa. The deposition of the films was done with three separate 2 in. elemental targets, with a purity of 99.999% for carbon (Demaco-Holland), 99.95% for Nb (AJA International-USA) and 99.995% for Ti (Kurt J. Lesker-USA), in a confocal configuration at a pressure of 0.25 Pa of pure Ar. The substrate bias voltage and substrate holder heating facility were turned off during depositions; the distance between target and substrates was about 15 cm. Prior to deposition, the substrates were sputter-cleaned with a negative bias of 180 V (25 W) in a 4 Pa Ar atmosphere for 10 min. The a-C film was deposited by applying a d.c. power of 380 W to the carbon target. The Nb−C film was deposited by applying simultaneously a d.c. power of 380 W and r.f. power of 100 W to the C and Nb targets, respectively. To improve the adhesion of the a-C and Nb−C films to the substrates, a pure Nb layer of ∼30 nm was deposited onto the substrates at a Nb target r.f. power of 230 W. TiO_2 films were deposited in an Ar/O_2 atmosphere (10 sccm Ar + 20 sccm O_2) at a total pressure of 0.4 Pa and applying a d.c. power of 230 W to the Ti target.

Chemical and Structural Characterizations. Film thicknesses were estimated by a quartz crystal microbalance (QCM) thickness monitor installed in the deposition chamber and the deposition rate was obtained by dividing the thickness by the deposition time. Before the final deposition, the QCM was calibrated based on the film thickness measured by scanning electron microscopy (SEM) using the cross-sectional film. The thickness of the a-C and Nb−C films was about 0.2 μm whereas that for the TiO_2 film was about 0.1 μm.

The surface topography of the films was observed by atomic force microscopy (AFM, Nanoscope V Multimode Atomic Force Microscope, Bruker) on an area of 1 × 1 μm. Images were acquired in contact mode using oxide-sharpened silicon nitride tips.

X-ray photoelectron spectroscopy (XPS) analyses were performed by means of a SAGE HR100 (SPECS) with a nonmonochromatic source (Al Kα 1486.6 eV) after a short etching of the samples surface in order to remove contamination.

Mechanical Characterization. Nanohardness, Young's modulus and elastic recovery of the films were measured by nanoindentation (Hysitron TI 950 TriboIndenter) using a Berkovich diamond indenter at different loads. The elastic recovery of the samples was determined as the percentage of the residual imprint compared to the total displacement of the load−displacement curves. At least 10 different measurements were done on each sample. The data were presented as mean ± standard deviation (SD).

Electrochemical Characterization. The electrochemical properties of the samples were measured by Tafel polarization using a Gamry unit, model PCI 4. The electrochemical tests were performed at 37 °C in Hank's solution (Hanks balanced salt solution, Sigma-Aldrich). The cell used for the experiments was composed of a platinum counter-electrode, a reference electrode of Ag/AgCl and a working electrode of film coated AISI 316 LVM steels substrates with an exposed area of 1 cm^2. Tafel polarization curves were obtained after 1 h of immersion in the solution, with a sweep step of 1 mV/s in a voltage range from −0.25 $V_{Ag/AgCl}$ to +0.25 $V_{Ag/AgCl}$. Corrosion rates were calculated from the slopes of the Tafel curves and the values of current density in the voltage range of ±0.25 V.

Cell Culture, Adhesion and Proliferation. MC3T3-E1 cells were used to evaluate the biocompatibility and bioactivity of the produced films. Cell culture and cell seeding on the films were performed as previously described.[17,18] Briefly, cells were cultured using α-MEM supplemented with 10% fetal bovine serum and 1% penicillin/streptomycin at 37 °C in an atmosphere of 5% CO_2. The culture medium was refreshed every 3 days. When the cells reached 80% confluence, they were trypsinized and resuspended in fresh medium to make a cell suspension with a final cell density of 3×10^4 cells/mL. 1 mL of cell suspension was added into each well of 24-well cell culture plates with film samples inside. After culturing for 3 h, cells were fixed in a 4% paraformaldehyde solution. For confocal laser scanning microscopy (CLSM, preformed on Zeiss LSM 510) observation, the F-actin, nucleus and focal adhesion of the cells were stained with actin cytoskeleton and focal adhesion staining kit (FAK100, Millipore). Briefly, cells cultured on the surface of the films were first permeabilized with Triton-X100 (Sigma, USA) for 4 min at room temperature. Then, the cells were incubated in dilute primary antibody (anti-vinculin) solution for 1 h at room temperature, followed by three times wash for 5−10 min each with phosphate buffered saline (PBS), followed by 1 h further incubation with secondary antibody fluorescein isothiocyanate (FITC)-conjugated and tetramethylrhodamine (TRITC)-conjugated Phalloidin at room temperature. After three times wash with PBS, cells were incubated with 4′,6-diamidino-2-phenylindole (DAPI) for 3 min at room temperature, followed by three times wash. For alkaline phosphatase (ALP) staining, the cells were seeded with a density of 4×10^4 cells/mL. After culturing for 14 days, cells were fixed 4% paraformaldehyde solution, and then stained with an ALP staining kit (1-Step TM NBT/BCIP, Thermo) for 1 h.

Statistical Analysis. For statistical analysis, SPSS 17.0 program was used, and the data were expressed as mean ± SD. Levene's test was performed to determine the homogeneity of variance for all the data. Tukey HSD post hoc tests were used for the data with homogeneous variance. Tamhane's T2 post hoc was employed in the case that the tested group did not have a homogeneous variance. A p-value of less than 0.05 was considered significant.

RESULTS AND DISCUSSION

The chemical composition of the films was studied by XPS based on the relative areas of the different photoelectron peaks. The XPS survey spectra of the samples are shown in Figure 1 and the chemical compositions are listed in Table 1. The film formed from sputtering using a single target of C (a-C) is composed of almost 100 at. % carbon, whereas the film incorporated with Nb film (Nb−C) is composed of around 39 at. % carbon and 52 at. % niobium. The TiO_2 film shows a composition of around 29 at. % titanium (Ti) and 63 at. % oxygen (O), with a Ti/O ratio close to the stoichiometric ratio of TiO_2.

Figure 2 shows typical three-dimensional AFM images (Figures 2A−C) of the surface topography of the film. All samples present nanoscale topographic features with root-mean-square (RMS) roughnesses below 1.55 nm, as shown in Table 1. Among these samples, the a-C film exhibits the lowest surface roughness (Figure 2 and Table 1), and the TiO_2 film

DOI: 10.1021/acsami.5b01193
ACS Appl. Mater. Interfaces 2015, 7, 6351−6358

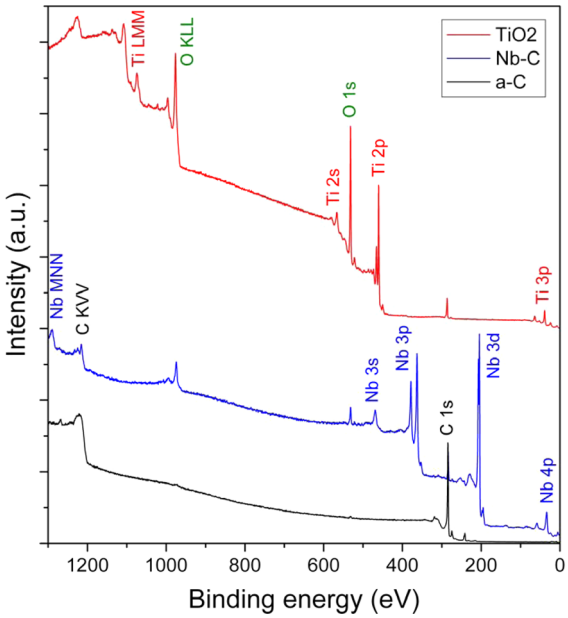

Figure 1. XPS survey spectra of the Nb−C, a-C and TiO_2 films.

exhibits the highest roughness, whereas the Nb−C film shows an intermediate roughness. Figure 2D−F show the representative top view AFM images of the films. Compared to other samples, the a-C film has the largest grains, with an average size of around 50 nm. By contrast, the Nb−C film shows smaller grains with an average size of around 17 nm, close to that for TiO_2 films. In our previous work, we proved that the Nb−C film exhibited a nanocomposite structure where the Nb−C nanosized crystals were embedded in an amorphous carbon matrix.[20] In summary, the introduction of Nb into the a-C films not only changes the surface chemistry, but also significantly alters the surface topography at nanoscale by tailoring the grain size and surface roughness (Figure 2).

Figure 3 shows the load−displacement nanoindentation curves for the a-C and the Nb−C films. The hardness and Young's modulus calculated based on these curves using the method proposed by Oliver and Pharr[21] are listed in Table 1. The hardness values for the a-C films are around 12 GPa. It is noted that the Nb−C films have a hardness as high as 22.5 GPa, significantly higher than the nanohardness of reported values for TiO_2 films, between 7 and 11 GPa,[19] and Ti-6Al-4 V alloys, around 4−5 GPa.[22] From Table 1, we can see that Nb−C film also has the highest elastic modulus (191.7 GPa), also much higher than those reported values of TiO_2 thin films[19] and Ti alloys.[22] The hardness values of the Nb−C films obtained in our study are comparable to those reported for other NbC films deposited by nonreactive[23] and reactive magnetron sputtering,[24] with maximum hardness values of around 22−24 GPa. More importantly, from the load−displacement curves, it can be seen that the elastic recovery percentages of Nb−C film and a-C film after deformation are 85% and 81%, respectively, suggesting that the Nb−C film exhibits a slightly better superelastic recovery behavior than the a-C film. Super elastic properties are of special interest in medical applications due to the large strains and deformations at which implants, stents or bone staples are subjected.[25] These results indicate that introduction of Nb into the a-C films can maintain and even slightly improve the superelasticity of the a-C film, and meanwhile improve the nanohardness and the Young's modulus.

Figure 4 presents potentiodynamic polarization curves of Nb−C, a-C and TiO_2 films. The corrosion potential (E_{corr}), corrosion current density (I_{corr}) and corrosion rate of the films are listed in Table 2. The E_{corr}, the open circuit potential of a corroding material, is one of the important indicators of the corrosion resistance of the films. In general, the more electropositive the E_{corr} is, the nobler or the less active the films are. From Table 2, it can be seen that the a-C was the noblest film, followed by the TiO_2 and the Nb−C films, and the latter two have a comparable E_{corr}. It is remarkable that the deposited Nb−C films in this work present a more electropositive E_{corr} values of −0.24 V, compared to those reported values in the range of −0.38 to −0.91 V for other Nb−C films.[26]

Corrosion rate of the film is another important index of the corrosion resistance of the film samples. It can be calculated according to eq 1,[27] based on I_{corr}, determined from the extrapolated slopes of the polarization curves. In general, low corrosion rates indicate better corrosion resistance. The calculated corrosion rates of the films, listed in Table 2, show that the TiO_2 and the Nb−C films have lower corrosion rates, compared to that of the a-C sample.

$$\text{corrosion rate} = \frac{0.13 \cdot I_{corr} \cdot EW}{d} \quad (1)$$

Here, EW and d correspond to the equivalent weight and density of the corroding species, respectively.

The higher corrosion rate of the a-C sample may be related to micropores in the structure, which can be observed in the AFM image (Figure 2E). On the other hand, the anticorrosion performance of the Nb−C films, similar to the TiO_2 films, can be attributed to their nanocomposite structure. The corrosion of orthopedic metal implants in human body has been widely studied. It is well-known that Cl^- ions in the physiological fluid are one of the most important factors for metal corrosion.[28] In this study, Hank's solution, a solution made to a physiological pH and salt concentration, was used for the anticorrosion tests. It is supposed that the Cl^- ions in the testing solution move with more difficulty across the Nb−C film to reach the underlying metal substrates and cause less film breakdown due to the dense nanocomposite structure of the film where the NbC nanocrystals are embedded in an amorphous carbon matrix.[20] An analog behavior have been seen in other

Table 1. Chemical Compositions Obtained from XPS Analysis, Root-Mean-Square (RMS) Roughness Obtained from AFM Measurement and Mechanical Properties Measured by Nanoindentation

sample	Nb (at. %)	Ti (at.%)	C (at. %)	O (at. %)	RMS roughness (nm)	hardness (GPa)	Young's modulus (GPa)
Nb−C	52.1		39.0	9.0	1.20	22.5 ± 0.5	191.7 ± 5.7
a-C			99.3	0.7	0.79	12.0 ± 0.3	96.6 ± 2.0
TiO_2		28.9	7.7	63.4	1.55	7−11[a]	80−120[a]

[a]Values obtained from the work of Jung et al.[19]

DOI: 10.1021/acsami.5b01193
ACS Appl. Mater. Interfaces 2015, 7, 6351−6358

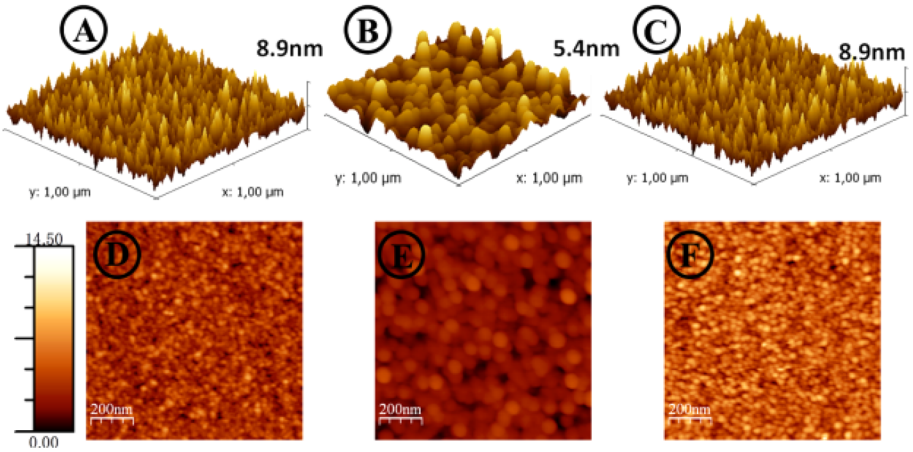

Figure 2. AFM images of (A, D) Nb−C, (B, E) a-C and (C, F) TiO_2 samples. The top three images (A, B and C) are three-dimensional AFM images and the bottom images (D, E and F) are the representative AFM top view images.

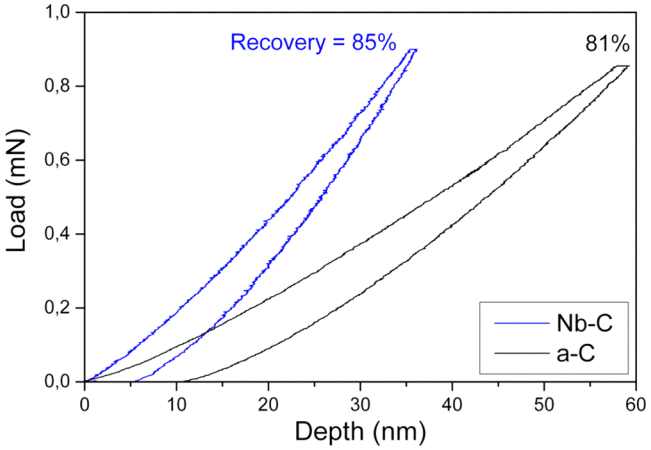

Figure 3. Load−displacement nanoindentation curves of the Nb−C and a-C films. The high elastic recovery of the Nb−C and a-C films can be appreciated.

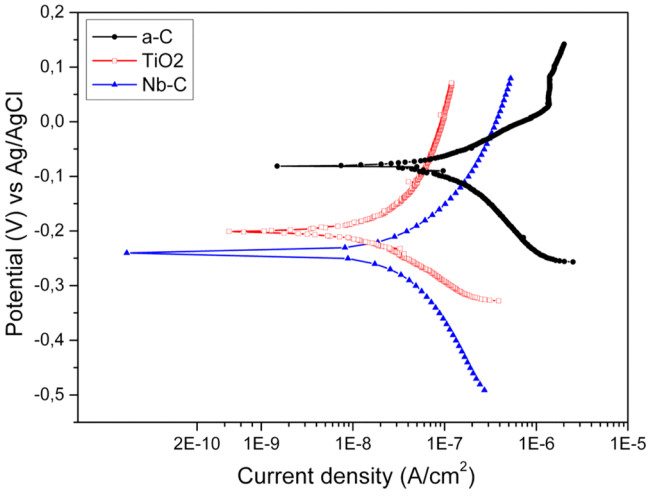

Figure 4. Polarization curves of the Nb−C, a-C and TiO_2 films.

nanostructured[29] and multilayered systems[30] where the interfaces limit the movement of Cl^- ions from the media to the underlying substrates.

The initial adhesion of cells on biomaterials is a key regulator of cell proliferation, migration and differentiation, which

Table 2. Values Obtained from the Polarization Curves of the Nb−C, a-C and TiO_2 Films

sample	$-E_{corr}$ (V)	I_{corr} (A·cm^{-2})	corrosion rate (mpy)
Nb−C	0.24	3.9×10^{-8}	0.017
a-C	0.08	2.1×10^{-7}	0.095
TiO_2	0.20	2.9×10^{-8}	0.013

determines the fate of the biomaterial. We used MC3T3-E1 cells, an osteoblast precursor cell line, to evaluate the cell adhesion on the film samples. Figure 5 shows the AFM images of the cells after culturing for 3 and 24 h on the Nb−C, a-C and TiO_2 films. From the images, we can clearly see the cell contour and topography. The cell nuclei can as well be recognized as the highest area in the cells, which is showed in the images in a bright color. After 3 h of culture, the cells cultured on all the films already partially flatten, showing a satellite-shaped morphology with cellular protrusions (lamellipodia and filopodia) extending from cell bodies to explore the underneath substrates. At 24 h, cells on all the films become fully flattened and their morphologies change from satellite shapes to polygonal shapes with different degrees of elongation, which are a characteristic morphology of osteoblasts. From the higher magnification images, we can clearly see the filopodia of the osteoblasts (Figure 5C,F,I).

Figure 6 shows the confocal laser scanning microscope images of the cells cultured on the Nb−C, a-C and TiO_2 films for 24 h. The nucleus (blue), F-actin (red) and vinculin (green) were stained and are shown in the second, third and fourth row in Figure 6, whereas the merged images are shown in the first row. From the images of F-actin, it can be seen that cells cultured on the Nb−C and a-C films share a similar size and exhibit obvious rearranged cytoskeleton with distinctive stress fibers inside the cytoplasm, especially at the border of the cells. By contrast, the size of the cells cultured on the TiO_2 film varied significantly: some of them are large in size with distinctive actin networks, whereas some of them have a smaller size showing a diffuse cytoskeleton with less obvious stress fibers in their cytoplasma. In the image of vinculin staining, more green spots can be found at the border of the cells cultured on the Nb−C film, compared to the cells cultured on the other films. In addition, we can also see some peri-nucleus regions showing a bright green color in the cells cultured on the Nb−C films. These results indicate enhanced focal adhesion of

DOI: 10.1021/acsami.5b01193
ACS Appl. Mater. Interfaces 2015, 7, 6351−6358

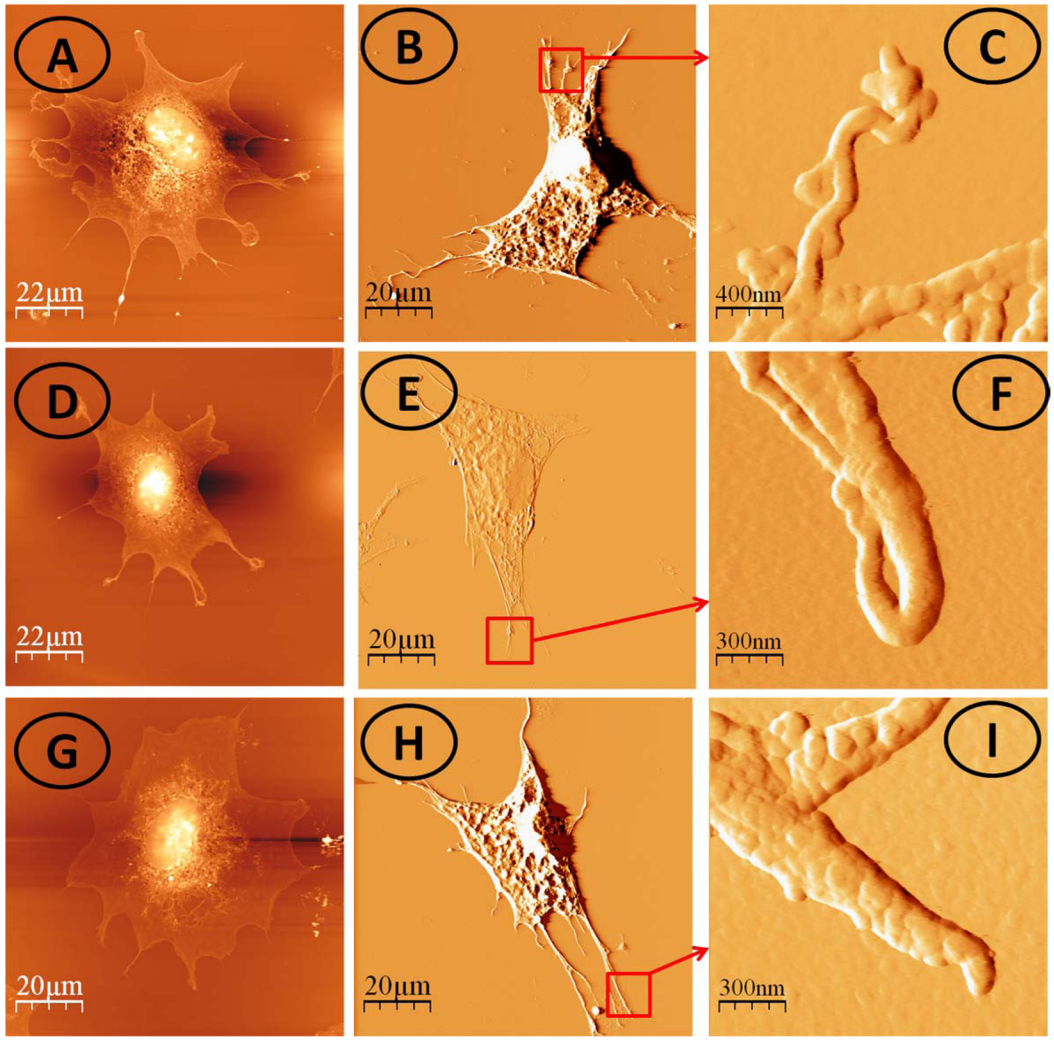

Figure 5. AFM images of the cells cultured on the Nb−C (A-C), a-C (D-F) and TiO_2 (G-I) films for 3 h (A, D and G) and 24 h (B, E and H). Images C, F and I are the higher magnification views of B, E and H, respectively.

cells on the Nb−C film sample. For the cells cultured on the a-C films, we can also see some green spots; however, much less can be found in the cells cultured on the TiO_2 films. From images of the cell nuclei, we can see that some of the nuclei show a round shape and other exhibit an elongated shape. It can be found that a significantly larger percentage of cell nuclei have an elongated shape in the cells cultured on the Nb−C and a-C films, compared to those cultured on the TiO_2 films, indicating that the Nb−C film exerts more profound influence on the behavior of the osteoblasts. In summary, AFM and confocal microscope images revealed that osteoblasts can adhere well on all the film samples. However, it is noted that the Nb−C films are superior to the a-C and TiO_2 films in terms of the enhancement of cell adhesion embodied in the reorganized cytoskeleton, formation of stress actin fibers and elongation of the nuclei. Similar effects of Nb on the morphology of bone-related cells were also found in other studies. Olivares Navarrete et al.[31] investigated the biocompatibility of Nb films prepared by magnetron sputtering on the stainless steel substrates and they found that human alveolar bone-derived cells cultured on the Nb films assumed elongated fibroblastic appearance, while those cultured on the stainless steel exhibited round shapes, indicating the influence of Nb on the behavior of bone-related cells.

Cells sense chemical and topographical cues in their surrounding microenvironment. These cues can be converted into intracellular signals and transduced to the nucleus in order to respond and adapt its functions.[32,33] Therefore, the cytoskeleton and nuclei morphology can be modulated by simply changing the surface chemistry and topography of the underlying substrates. In this study, the addition of Nb to the a-C film not only changed the surface chemistry but also altered the nanotopography of the film, which can be the reasons for the better interaction of the nanocomposite Nb−C films with osteoblasts.

The proliferation of the cells cultured on the Nb−C, a-C and TiO_2 films was also evaluated, and the result is displayed in Figure 7. Cells cultured in the wells of the cell culture plate without film samples were also used as a control group in this assay. It can be seen that at both time points (3 days and 7 days) cells cultured on the films have a higher proliferation rate than those cultured on the cell culture plates ($P < 0.05$). The average proliferation rates of the cells cultured on the Nb−C and a-C films are higher without significant difference, compared to the cells cultured on the TiO_2 films. This result indicates that all the film samples can promote the cell proliferation.

DOI: 10.1021/acsami.5b01193
ACS Appl. Mater. Interfaces 2015, 7, 6351−6358

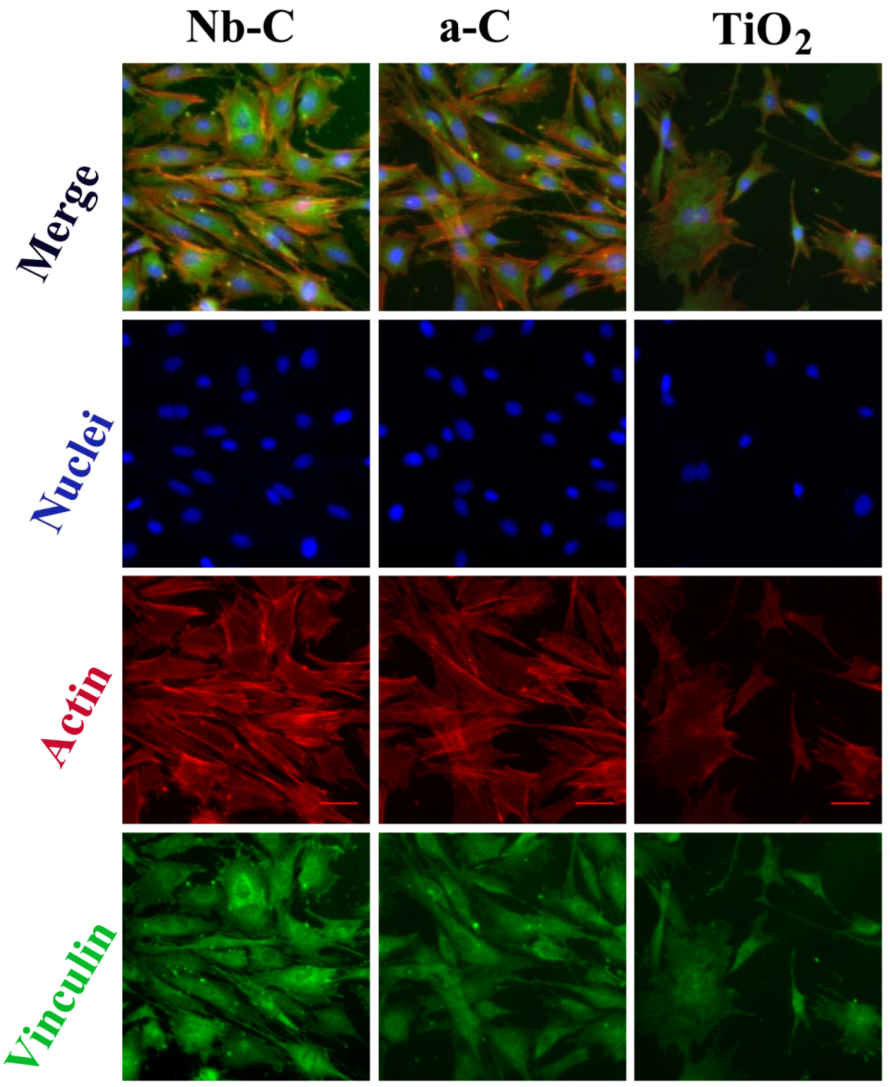

Figure 6. Confocal laser scanning microscope images of the cells cultured on the Nb−C, a-C and TiO_2 films for 24 h: the nucleus (blue), F-actin (red) and vinculin (green).

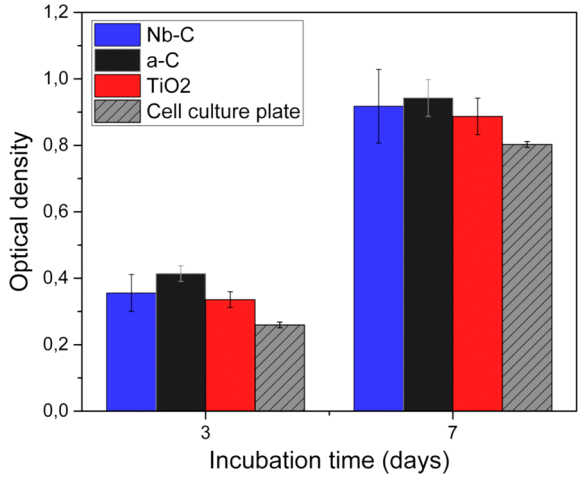

Figure 7. Proliferation of cells cultured on the Nb−C, a-C and TiO_2 films for 3 and 7 days.

In this study, we also evaluate ALP activity of the osteoblasts cultured on the film samples. ALP activity is one of the gene markers in the early stage of the osteogenic differentiation. Figure 8 shows the ALP activity of the cells cultured on the Nb−C, a-C and TiO_2 films. More cells cultured on the Nb−C films after staining exhibit a darker blue color, compared to those cultured on the other two films, especially on the TiO_2 film. These results indicate that the cells cultured on the Nb−C film have enhanced ALP activity compared to those on the a-C film and the TiO_2 film, implying the positive effects of Nb on the osteoblast differentiation ability. The enhancement on the ALP activity by the Nb has been reported by others. Shapira et al.[15] reported that osteoblasts cultured on Ti-6Al-7Nb showed enhanced ALP activity, higher expression levels of osteocalcin and transforming growth factor, compared to those cultured on the currently used Ti-6Al-4 V.

In summary, we, in this study, successfully "bioactivate" the bioinert carbon films by the incorporation of Nb. As indicated by the results, the addition of Nb not only changes the surface chemistry of the a-C films, but also led to the refinement of the nanotopography of the film (Figure 2), which are supposed to jointly contribute to the enhancement on the cell adhesion and the increase in the ALP activity. It is known that there is a thin TiO_2 layer caused by the natural oxidation on the outmost layer of the Ti based alloy implants, which can enhance the corrosion

DOI: 10.1021/acsami.5b01193
ACS Appl. Mater. Interfaces 2015, 7, 6351−6358

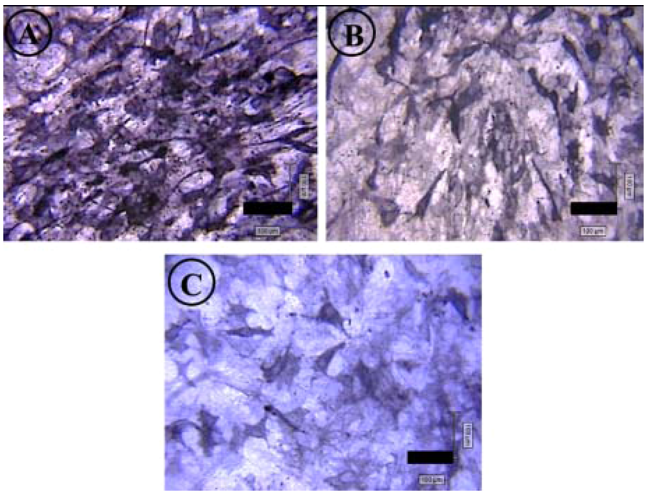

Figure 8. ALP staining of cells cultured on the Nb−C (A), a-C (B) and TiO_2 (C) films for 14 days.

resistance and biocompatibility of the implants.[34] Therefore, we choose TiO_2 films as a control group in this study for comparison. Besides the better biological performance, our developed Nb−C films also possess better nanomechanical properties and comparable corrosion resistance compared to the TiO_2 films. This indicates the potential of the Nb−C nanocomposite films for orthopedic applications.

CONCLUSIONS

In this study, we incorporated Nb into the a-C films using nonreactive magnetron sputtering to endow implants with the ability to activate the functions of bone-related cells. The a-C films show a lower nanoroughness and larger grains, which are increased and decreased, respectively, after addition of Nb. The newly formed Nb−C films show better mechanical properties in terms of nanohardness, Young's modulus and especially superelasticity, with around 85% elastic recovery. In vitro cell experiments using preosteoblasts (MC3T3-E1) revealed that the Nb−C films enhance the cellular adhesion and increase the expression of ALP activity of the cells cultured on their surfaces. Moreover, it is also found that the addition of Nb can significantly retard the corrosion of the underlying metal substrate. This study provides a strategy to bioactivate bioinert/biocompatible films for orthopedic applications and points out the potential significance of Nb in the enhancement on the bioactivity of the orthopedic implants.

AUTHOR INFORMATION

Corresponding Author

*Guocheng Wang. Phone: +34 943 00 53 21. E-mail: gwang@cicbiomagune.es.

Author Contributions

The paper was written through contributions of all authors. All authors have given approval to the final version of the paper.

Notes

The authors declare no competing financial interest.

ACKNOWLEDGMENTS

L. E. Coy thanks the financial support from the National Centre for Research and Development under research grant "Nanomaterials and their application to biomedicine", contract number PBS1/A9/13/2012. S. E. Moya, D. Gregurec and G. C. Wang thank the project MAT2013-48169-R from the Spanish Ministery of Economy (MINECO) for financial support. W. Aperador thanks the financial support from the Universidad Militar Nueva Granada, contract number ING-1775.

REFERENCES

(1) Geetha, M.; Singh, A. K.; Asokamani, R.; Gogia, A. K. Ti based Biomaterials, the Ultimate Choice for Orthopaedic Implants - A Review. *Prog. Mater. Sci.* **2009**, *54*, 397−425.

(2) Yoshinari, M.; Matsuzaka, K.; Inoue, T.; Oda, Y.; Shimono, M. Bio-functionalization of Titanium Surfaces for Dental Implants. *Mater. Trans.* **2002**, *43*, 2494−2501.

(3) Durmus, N. G.; Webster, T. J. Nanostructured Titanium: The Ideal Material for Improving Orthopedic Implant Efficacy? *Nanomedicine (London, U. K.).* **2012**, *7*, 791−793.

(4) Dohan Ehrenfest, D. M.; Coelho, P. G.; Kang, B.-S.; Sul, Y.-T.; Albrektsson, T. Classification of Osseointegrated Implant Surfaces: Materials, Chemistry and Topography. *Trends Biotechnol.* **2010**, *28*, 198−206.

(5) Wang, G.; Meng, F.; Ding, C.; Chu, P. K.; Liu, X. Microstructure, Bioactivity and Osteoblast Behavior of Monoclinic Zirconia Coating with Nanostructured Surface. *Acta Biomater.* **2010**, *6*, 990−1000.

(6) Yim, E. K. F.; Darling, E. M.; Kulangara, K.; Guilak, F.; Leong, K. W. Nanotopography-Induced Changes in Focal Adhesions, Cytoskeletal Organization, and Mechanical Properties of Human Mesenchymal Stem Cells. *Biomaterials* **2010**, *31*, 1299−1306.

(7) Zhao, X.; Wang, G.; Zheng, H.; Lu, Z.; Zhong, X.; Cheng, X.; Zreiqat, H. Delicate Refinement of Surface Nanotopography by Adjusting TiO_2 Coating Chemical Composition for Enhanced Interfacial Biocompatibility. *ACS Appl. Mater. Interfaces* **2013**, *5*, 8203−8209.

(8) Roach, P.; Eglin, D.; Rohde, K.; Perry, C. C. Modern Biomaterials: A Review - Bulk Properties and Implications of Surface Modifications. *J. Mater. Sci.: Mater. Med.* **2007**, *18*, 1263−1277.

(9) Dearnaley, G.; Arps, J. H. Biomedical Applications of Diamond-like Carbon (DLC) Coatings: A Review. *Surf. Coat. Technol.* **2005**, *200*, 2518−2524.

(10) Tiainen, V. M.; Soininen, A.; Alakoski, E.; Konttinen, Y. T. In Situ Surface Oxide Reduction with Pulsed Arc Discharge for Maximum Adhesion of Diamond-like Carbon Coatings. *Diamond Relat. Mater.* **2008**, *17*, 2071−2074.

(11) Dalstra, M.; Denes, G.; Melsen, B. Titanium-Niobium, a New Finishing Wire Alloy. *Clin. Orthod. Res.* **2000**, *3*, 6−14.

(12) Xu, J.; Weng, X. J.; Wang, X.; Huang, J. Z.; Zhang, C.; Muhammad, H.; Ma, X.; Liao, Q. De. Potential Use of Porous Titanium-Niobium Alloy in Orthopedic Implants: Preparation and Experimental Study of Its Biocompatibility in Vitro. *PLoS One* **2013**, *8*.

(13) Osathanon, T.; Bespinyowong, K.; Arksornnukit, M.; Takahashi, H.; Pavasant, P. Ti-6Al-7Nb Promotes Cell Spreading and Fibronectin and Osteopontin Synthesis in Osteoblast-like Cells. *J. Mater. Sci.: Mater. Med.* **2006**, *17*, 619−625.

(14) Challa, V. S. A.; Mali, S.; Misra, R. D. K. Reduced Toxicity and Superior Cellular Response of Preosteoblasts to Ti-6Al-7Nb Alloy and Comparison with Ti-6Al-4V. *J. Biomed. Mater. Res., Part A* **2013**, *101 A*, 2083−2089.

(15) Shapira, L.; Klinger, A.; Tadir, A.; Wilensky, A.; Halabi, A. Effect of a Niobium-Containing Titanium Alloy on Osteoblast Behavior in Culture. *Clin. Oral Implants Res.* **2009**, 578−582.

(16) Zhao, X.; Wang, G.; Zheng, H.; Lu, Z.; Cheng, X.; Zreiqat, H. Refining Nanotopographical Features on Bone Implant Surfaces by Altering Surface Chemical Compositions. *RSC Adv.* **2014**, *4*, 54226−54234.

(17) Wang, G.; Lu, Z.; Xie, K. Y.; Lu, W. Y.; Roohani-Esfahani, S. I.; Kondyurin, A.; Zreiqat, H. A Facile Method to in Situ Formation of Hydroxyapatite Single Crystal Architecture for Enhanced Osteoblast Adhesion. *J. Mater. Chem.* **2012**, *22*, 19081.

(18) Wang, G.; Lu, Z.; Zhao, X.; Kondyurin, A.; Zreiqat, H. Ordered HAp Nanoarchitecture Formed on HAp−TCP Bioceramics by

DOI: 10.1021/acsami.5b01193
ACS Appl. Mater. Interfaces 2015, 7, 6351−6358

"nanocarving" and Mineralization Deposition and Its Potential Use for Guiding Cell Behaviors. *J. Mater. Chem. B* **2013**, *1*, 2455.
(19) Jung, H.; Park, C.; Lee, J.; Park, Y. S. Tribological and Electrical Properties of TiO_2 Thin Films for Polymer Insulator as the Dielectric Coating of Electric Railroad. *Mater. Res. Bull.* **2014**, *58*, 44−48.
(20) Yate, L.; Coy, L. E.; Wang, G.; Beltrán, M.; Díaz-Barriga, E.; Saucedo, E. M.; Ceniceros, M. A.; Zaleski, K.; Llarena, I.; Möller, M.; Ziolo, R. F. Tailoring Mechanical Properties and Electrical Conductivity of Flexible Niobium Carbide Nanocomposite Thin Film. *RSC Adv.* **2014**, *4*, 61355−61362.
(21) Oliver, W.; Pharr, G. An Improved Technique for Determining Hardness and Elastic Modulus Using Load and Displacement Sensing Indentation Experiments. *J. Mater. Res.* **1992**, *7*, 1564−1583.
(22) Murr, L.; Quinones, S.; Gaytan, S.; Lopez, M.; Rodela, A.; Martinez, E.; Hernandez, D.; Martinez, E.; Medina, F.; Wicker, R. Microstructure and Mechanical Behavior of Ti-6Al-4V Produced by Rapid-Layer Manufacturing, for Biomedical Applications. *J. Mech. Behav. Biomed. Mater.* **2009**, *2*, 20−32.
(23) Nedfors, N.; Tengstrand, O.; Lewin, E.; Furlan, A.; Eklund, P.; Hultman, L.; Jansson, U. Structural, Mechanical and Electrical-Contact Properties of Nanocrystalline-NbC/Amorphous-C Coatings Deposited by Magnetron Sputtering. *Surf. Coat. Technol.* **2011**, *206*, 354−359.
(24) Zhang, K.; Wen, M.; Cheng, G.; Li, X.; Meng, Q.; Lian, J.; Zheng, W. Reactive Magnetron Sputtering Deposition and Characterization of Niobium Carbide Films. *Vacuum* **2014**, *99*, 233−241.
(25) Zheng, Y.; Zhang, B.; Wang, B.; Wang, Y.; Li, L.; Yang, Q.; Cui, L. Introduction of Antibacterial Function into Biomedical TiNi Shape Memory Alloy by the Addition of Element Ag. *Acta Biomater.* **2011**, *7*, 2758−2767.
(26) Braic, M.; Braic, V.; Balaceanu, M.; Vladescu, A.; Zoita, C.; Titorencu, I.; Jinga, V.; Miculescu, F. Preparation and Characterization of Biocompatible Nb−C Coatings. *Thin Solid Films* **2011**, *519*, 4064−4068.
(27) Stern, M. A Method for Determining Corrosion Rates from Linear Polarization Data. *Corrosion* **1958**, *14*, 440t−444t.
(28) Virtanen, S.; Milošev, I.; Gomez-Barrena, E.; Trebše, R.; Salo, J.; Konttinen, Y. T. Special Modes of Corrosion under Physiological and Simulated Physiological Conditions. *Acta Biomater.* **2008**, *4*, 468−476.
(29) Kok, Y.; Hovsepian, P. E. Resistance of Nanoscale Multilayer C/Cr Coatings against Environmental Attack. *Surf. Coat. Technol.* **2006**, *201*, 3596−3605.
(30) Moreno, H.; Caicedo, J.; Amaya, C.; Cabrera, G.; Yate, L.; Aperador, W.; Prieto, P. Improvement of the Electrochemical Behavior of Steel Surfaces Using a TiN[BCN/BN]n/c-BN Multilayer System. *Diamond Relat. Mater.* **2011**, *20*, 588−595.
(31) Olivares-Navarrete, R.; Olaya, J. J.; Ramírez, C.; Rodil, S. E. Biocompatibility of Niobium Coatings. *Coatings* **2011**, *1*, 72−87.
(32) Gittens, R. A.; Olivares-Navarrete, R.; Cheng, A.; Anderson, D. M.; McLachlan, T.; Stephan, I.; Geis-Gerstorfer, J.; Sandhage, K. H.; Fedorov, A. G.; Rupp, F.; Boyan, B. D.; Tannenbaum, R.; Schwartz, Z. The Roles of Titanium Surface Micro/Nanotopography and Wettability on the Differential Response of Human Osteoblast Lineage Cells. *Acta Biomater.* **2013**, *9*, 6268−6277.
(33) Burdick, J. A.; Vunjak-Novakovic, G. Engineered Microenvironments for Controlled Stem Cell Differentiation. *Tissue Eng., Part A* **2009**, *15*, 205−219.
(34) Velten, D.; Biehl, V.; Aubertin, F.; Valeske, B.; Possart, W.; Breme, J. Preparation of TiO2 Layers on Cp-Ti and Ti6Al4V by Thermal and Anodic Oxidation and by Sol-Gel Coating Techniques and Their Characterization. *J. Biomed. Mater. Res.* **2002**, *59*, 18−28.

DOI: 10.1021/acsami.5b01193
ACS Appl. Mater. Interfaces 2015, 7, 6351−6358